Odorant molecular feature mining by diverse deep neural networks for prediction of odor perception categories

Liang Shang[1,2,*], Chuanjun Liu[3,4], Fengzhen Tang[1,2,*] ,Bin Chen[5], Lianqing Liu[1,2], Kenshi Hayashi[3]

[1] State Key Laboratory of Robotics, Shenyang Institute of Automation, Chinese Academy of Sciences, Shenyang, 110016, China

[2] Institute for Robotics and Intelligent Manufacturing, Chinese Academy of Sciences, Shenyang, 110016, China

[3] Department of Electronics, Graduate School of Information Science and Electrical Engineering, Kyushu University, Fukuoka, 819-0395, Japan

[4] Research Laboratory, U.S.E. Co., Ltd., Tokyo, 150-0013, Japan

[5] Chongqing Key Laboratory of Non-linear Circuit and Intelligent Information Processing, College of Electronic and Information Engineering, Southwest University, Chongqing, 400715, China

*Corresponding Author(s): Liang Shang (shangliang0225@gmail.com), Fengzhen Tang (tangfengzhen@sia.cn)

Abstract

The prediction of structure-odor-relationship (SOR) by deep neural networks (DNN) via the structural features of odorants has attracted great attention during the past decade. Due to the limited knowledge on binding mechanism between odorant molecules and olfactory receptors, however, it is not sure what kind of structural features play the most important role in smell recognition. Here, diverse DNNs, including molecular parameters neural network, molecular graphic convolution neural network (MG-CNN), molecular graph transformer neural network, and atom interaction neural network, were used to extract the structure features of molecules and to predict the categorized odor perception. The experimental results demonstrated that an MG-CNN combined with a multi-label DNN classifier produced the best results, with an area under the receiver operating characteristic curve and F1-score of 0.877±0.028 and 0.726±0.028, respectively. This is the first systematic study for molecular structure features extracted by different deep neural network and their predictive effect for SOR. We believe that these insights regarding the use of DNN-based odorant molecular feature extraction for odor sensory identification will be useful for introducing biologically interpretable artificial intelligence into olfactometry, and thus contribute to our understanding of the mechanisms underlying human olfaction.

Keywords

Odor sensory category, Structure odor relationship, Odorant molecules structure features extraction, Machine learning, Recognition and classification

Introduction

Identifying the interactions between odorants and sensory descriptions is important for the discovery and analysis of volatile compounds. To obtain the sensory information of odor, gas chromatography/olfactometry (GC/O) has been widely applied as a powerful odor analytic strategy in various research areas, such as agriculture, food, and environmental science[1, 2]. In addition, gas separation membranes had been developed successfully forGC part[3, 4]. Although GC/O can be used to attain accurate sensory and chemical characteristics of odorants, this approach is expensive and time-consuming, which can limit its application. The main expense associated with GC/O is the cost of hiring and training panelists to characterize the sensory qualities of odorants using their sense of smell. In addition, the sensory assessment of human panelists is personally dependent, which inevitably leads to subjectivity and inconsistency into the evaluation results.

Research on the response patterns of neurons in the olfactory bulbs (OB) has illuminated the mechanisms underlying biological olfaction[5, 6]. However, many questions remain, such as why these molecules smell different from one another and why we link smell feelings with certain semantic descriptors, known as odor descriptors (ODs). These questions may be answered by examining structure odor relationships (SORs), the development of which presents a difficult and interesting challenge[7, 8]. During recent years, many researches have been conducted to predict odor perception of odorants using vairous parameters, such as electronic or physicochemical characteristics[9-11], mass spectrometry (MS)[12], and social network interactions[13]. Additionally, novel methods, such as odor-based social networks[14-16], machine learning (ML)[17-19], deep neural network (DNN) models[20-22], and semantic-based approaches[23] have been developed to calibrate models that express the relationships between odorants and ODs. These studies have demonstrated the possibility to use data-driven approaches to solve the SOR problems. In line with this trend, we have proposed a concept of ML-based GC/MS olfactometry in which the sensory evaluation of panelists is expected to be replaced by machine learning prediction models[24].

In the ML-based GC/O system, the molecular information obtained by MS analysis of the individual GC peaks is transfered into physicochemical parameters by molecular calculation software (DRAGON). By building models appropriately, the ODs of the odorants can be predicted with high accuracy form their physicochemical parameters. The ML-based GC/O is a concept-of-proof study and there are many problems to be solved before its practical application. For example, in terms of the sample size, only limited ODs with high frequency of occurrence are targeted in our models. In reality, it has been reported that over 500 ODs are used for odor evaluation[25]. Therefore, many ODs, especially for those rare ODs are not considered by the models. In oder to solve this issue, we have recently proposed a categorization approach based on the semantic analysis of ODs, which make the model can cover the prediction of several hundreds of ODs[26]. Another remaining problem is that the model prediction is based on physicochemical parameters of odorants. The recent development of computational chemistry and ML make it possible to obtain various molecular structure information[27]. Unlike traditional methods, DNNs can directly learn latent presentations from molecular structures, such as atom types and their positions, via back-propagation[28]. Moreover, an end-to-end strategy has been proposed as an effective nonlinear modeling method for learning molecular presentation in many fields, such as quantum chemical properties prediction, and compound-protein interaction identification[29]. However, since detailed binding mechanism between the odorants and olfactory receptors is still not fully understood, which molecular features play the most important role in olfactory perception has not been cleared.

The purpose of this study is dedicated to molecular feature mining by diverse DNNs for prediction of odor perception categories. Please note that our work is not to propose some novel classification frameworks, but using multi-type of feature extractors to understand the relationship between the structure features of odorants and odor perception categories. A schematic of the data processing and modeling procedures is illustrated in Figure 1. We used molecular structures, including 2D molecular images and atom spatial locations, to predict odor sensory categories. For minding useful information from molecular structures, some molecular structural feature extraction methods were empoyed and their results were compared and discussed.

Specifically, we used a molecular graphic convolution neural network (MG-CNN) and molecular graph transformer neural network (MGTNN) to extract features from representations of molecular structure, such as molecular structure images and topology graphs. Moreover, we used atom interaction neural networks (AINNs) to generate features from the spatial structures of atoms. To overcome limitations related to insufficient samples, we also considered pre-trained models, such as pre-trained CNNs and MGTNNs. We compared the feasibility of SOR prediction via molecular fingerprints, molecular parameters, and molecular feature extraction based on MG-CNN, MGTNN, and AINN. We achieved the highest performance by applying molecular features extracted via a pre-trained MG-CNN combined with a mulit-label learning model (area under the ROC curve: 0.877±0.028 and F-score: 0.726±0.028). Thus, the proposed odor sensory category identification model is a feasible option for developing artificial intelligence (AI)-based GC/O. Although it would be still a challenge to replace human assessors by ML models perfectly, the proposed method could provide references for assessors to increase the efficiency for odor analysis. Therefore, the limitation of odor memory would be breaked through by the odor perception categories recommendated by the proposed method.

Materials and Methods

Data collection and preparation

To create an odor category prediction model, we collected an extensive dataset containing 2849 odorants. We used information from publicly available databases such as the Odor Map database[30], Flavors and Fragrances database (Sigma-Aldrich)[31], and the Good Scents database[32]. As illustrated in Figure 1, we collected and prepared 5 types molecular descriptors, including molecular parameters, molecular fingerprints, molecular graphs, simplified molecular input line entry system (SMILES), and atom coordinates. Specifically, we used SMILES and RDKit Software (ver. 2021.03.1)[33, 34] to collect normalized molecular parameters (1826, detailed information can be found at[35]), molecular fingerprints (binary, 2048 bits), and 2D molecular graphs (RGB, 300×300 pixels). We used RDKit to obtain the 2D and 3D atom coordinates of the odorants, which we used to

train the model regarding the atomic interactions between odorant structures and their odor sensory categories. In total, 256 ODs were clustered into 20 categories using a co-occurrence Bayesian embedding method. More detailed information regarding the cleaning and categorization of ODs can be found in Table S1[26]. Data were processed and analyzed using Python (ver. 3.9.0) and R (ver. 4.1.1). Because the diverse molecular representations of odorants, we need to employ various of feature extraction technologies to obtain embeddings for model calibration.

Model calibration

The calibration and validation process for the odor category model is shown in Figure 1. First, all samples were divided via random splitting into training and test sets with a 4:1 ratio, and the reported results are averaged over 50 repetitions. Afterward, we employed molecular parameters, molecular fingerprints, molecular graphic features, molecular graph transformers, and atomic interaction embedding to extract the molecular features of the odorants (Figure 2). We used a DNN approach to develop a multi-label odor category learning model (the output size was 20) based on the aforementioned molecular information. The cost function $\mathcal{L}(\mathbf{\Theta})$ of the DNN multi-label classifier was calculated by summing the binary cross-entropy of each class, which was defined as follows:

$$\mathcal{L}(\mathbf{\Theta}) = \frac{1}{N}\sum_{i=1}^{N}\sum_{j=1}^{M} y_{i,j} \times \log(\hat{y}_{i,j}) + (1 - y_{i,j}) \times \log(1 - \hat{y}_{i,j}) \qquad \text{Equation 1}$$

where $\mathbf{\Theta}$ indicates the parameter set of the model, *N* indicates the sample number in the training set, and *M* indicates the number of odor categories, set as 20 in the present study. $y_{i,j}$ and $\hat{y}_{i,j}$ are the ground truth and prediction label for category *j* of sample *i*, respectively. By minimizing the cost function based on the stochastic steepest gradient descent algorithm, parameters from the DNN could be learned and updated. For each DNN method, the number of hidden layers and nodes was selected from 1 to 8 layers and {16, 32, 64, 128, 256, 512, 1024, 2048} nodes, respectively. Network parameters, including the dropout ratio, learning rate, and training

epoch, were set as 0.1, 1×10^{-4}, and 200, respectively. The optimal models were determined according to their areas under the ROC curve (AUC) and F-scores based on precision and recall, simultaneously. Both qualitative and quantitative data analyses were performed.

Because molecular graphs, molecular SMILES sequences, and atom coordinates are not tabular data, they cannot be used as classifier inputs directly. Therefore, diverse feature extraction methods were firstly employed to convert those unstructured data to tabular features. Specifically, pre-trained CNNs, sequence transformer, and atomic interaction embedding were utilized for moelcular graphs, SMILES sequences, and atom coordinates features extraction, respectively. Detail information of above-mentioned strategies were summarized as fllows.

Molecular graphic feature extraction

CNNs are highly successful graphic feature extractors, and are commonly developed with high accuracy by large training datasets[36]. Given the utility of convolution kernels and DNNs, CNNs have played a critical role in image and video processing[37]. Recently, molecular graph embedding has been used to model the relationships between chemical compounds[29]. To investigate the feasibility of molecular graphic presentation for odor category prediction, we used 4 types of effective CNNs, including the VGG-16, Restnet, Densnet, and Alexnet, as feature extractors for generating embedding from molecular images in the present study (Figure 2a). Detailed structures for these CNNs have been previously presented[38-41]. In the present study, we used pre-trained CNN models for odor category prediction to overcome the limitation of sample size.

Molecular sequence feature extraction

As an end-to-end supervised learning algorithm, graph neural networks (GNNs) have been widely applied for sequence embedding in various fields[42]. Given that odorants can be described as molecular topology graphs using SMILES, we considered GNNs to be appropriate for molecular presentation. Broadly speaking, graph transformers are considered to be a powerful tool for handling molecular presentation through encoding via

SMILES, which has been used to predict compound protein interactions, virtual screening, and molecular parameters[43].

Although the molecular graph transformer neural network (MGTNN) has strong potential for molecular modeling, deep learning models always require a large amount of labeled data for training[44]. To overcome the above problems, we used a self-supervised graph transformer (GROVER) to obtain presentation information from the odorants for odor category prediction. A briefly description of the GROVER is given in Figure 2b. The pre-training architecture was mainly composed of two parts: i) a transformer-based neural network, and ii) a GNN for molecular structure extraction. The input of the model was an odorant graph presentation $\mathcal{G} = (V, E)$, where *V* was the set of atoms and *E* was the set of bonds. Specifically, $v_i \in V$ and $e_{i,j} \in E$ were the *i*-th atom and bond between the *i*-th and *j*-th atom, respectively. The GNN was designed to embed extraction according to queries (**Q**), keys (**K**), and values (**V**) from the atoms in molecular graphs ($\mathcal{G}$). The message transmission process of the GNN, as well as the neighborhood aggression between an atom (*v*) and its neighbors ($\mathcal{N}_v$) in an odorant ($\mathcal{G}$), were adopted to iteratively (*L*) update hidden states ($\mathbf{h}_v$) for atom *v*, which can be written as:

$$\begin{aligned} \mathbf{m}_v^{(l,k)} &= \mathrm{Aggregate}^{(l)}(\{(\mathbf{h}_v^{(l,k-1)}, \mathbf{h}_u^{(l,k-1)}, \mathbf{e}_{v,u}) | u \in \mathcal{N}_v\}) \\ \mathbf{h}_v^{(l,k)} &= \sigma(\mathbf{W}^l \mathbf{m}_v^{(l,k)} + \mathbf{b}^{(l)}) \\ \mathbf{h}_{\mathcal{G}} &= \mathrm{Readout}(\{\mathbf{h}_v^{(0,K_0)}, \ldots, \mathbf{h}_v^{(L,K_L)} | v \in V\}) \end{aligned} \qquad \text{Equation 2}$$

where $\mathbf{m}_v^{(l,k)}$ indicates the passing message for atom *v* under the *k*-th step of the *l*-th iteration. Here, we suppose each iteration (*l*) contains K_l steps. $\mathrm{Aggregate}^{(l)}(\cdot)$ is an aggregation function, which can be selected from the mean, max pooling, or graph attention mechanism. $\sigma(\cdot)$ is the activation function, and $\mathbf{h}_{\mathcal{G}}$ is the graph-level representation generated by a $\mathrm{Readout}$ operation. The resulting matrices (**Q**, **K**, **V**) were fed to the transformer module, which was composed of graph multi-head attention blocks:

$$\begin{aligned} \mathrm{MultiHead}(\mathbf{Q}, \mathbf{K}, \mathbf{V}) &= \mathrm{concat}(\mathrm{head}_1, \mathrm{head}_2, \ldots, \mathrm{head}_k)\mathbf{W}^O \\ \mathrm{head}_i &= \mathrm{Attention}(\mathbf{Q}\mathbf{W}_i^Q, \mathbf{K}\mathbf{W}_i^K, \mathbf{V}\mathbf{W}_i^V) \\ \mathrm{Attention}(\mathbf{Q}, \mathbf{K}, \mathbf{V}) &= \mathrm{softmax}(\mathbf{Q}\mathbf{K}^T/\sqrt{d})\mathbf{V} \end{aligned} \qquad \text{Equation 3}$$

where $\mathbf{W}_i^{\mathbf{Q}}$, $\mathbf{W}_i^{\mathbf{K}}$, $\mathbf{W}_i^{\mathbf{V}}$ are the projection matrices of head_i. *d* indicates the dimension of **q** and **k**.

The self-supervised learning tasks in the present study were assigned as contextual property prediction, and graph-level motifs, as well as molecular components, were used to predict links between both nodes and edges. In summary, we employed a pre-trained model, calibrated with 10 million molecules, as a molecular topology feature extractor in the present study. Instances of atom embedding (2048 dimensions) and bond embedding (2048 dimensions) generated by the above-mentioned procedure were used for odor category prediction. This simple strategy has been demonstrated to be a powerful method in terms of graph expression and structure information extraction[45]. Details regarding graph transformers can be found elsewhere[46].

Atomic interaction embedding

Numerous studies have confirmed that atom interactions are crucial to odor perception[47, 48]. Consequently, molecular features generated by atomic interactions may be feasible for odor category prediction. In the present study, we modeled interactions between atoms in an odorant molecule using a DNN-based model as a molecular feature extractor. A brief description of the process for the AINN is given in Figure 2c. Formally, given an odorant $\mathcal{O} = \{(a_i, \mathbf{c}_i)\}_{i=1}^{\mathcal{N}_{atom}}$, where a_i is the *i*-th atom type, $\mathbf{c}_i \in \mathbb{R}^2 or \mathbb{R}^3$ is the coordinate vector of the *i*-th atom, and N_{atom} is the total number of atoms for the odorant. To obtain an atom embedding description for the odorant, $\mathcal{V}_{\mathcal{O}} = \{(\mathbf{v}_i, \mathbf{c}_i)\}_{i=1}^{\mathcal{N}_{atom}}$, where $\mathbf{v}_i \in \mathbb{R}^d$ is the embedded vector for the *i*-th atom. The embedding dimensionality *d* is a hyper-parameter that must be assigned before training, and these atom embeddings were initialized randomly and optimized via back propagation. To select the update strategy for the above-mentioned embeddings, we referred to the previous use of DNNs with common graph-structured datasets[27, 49]. Accordingly, the atom embeddings were updated as follows:

$$
\begin{aligned}
\mathbf{v}_i^{(l+1)} &= f(\mathbf{v}_i^l) + \sum_{j \in \mathcal{O} \setminus i} g(\mathbf{v}_j^{(l)}, P_{i,j}^{(l)}, \alpha_{i,j}^{(l)}) \\
P_{i,j}^{(l)} &= f(\mathbf{v}_i^{(l)}, \mathbf{v}_j^{(l)}, dist_{i,j}) \\
\alpha_{i,j}^{(l)} &= f(\mathbf{v}_i^{(l)}, \mathbf{v}_j^{(l)}, dist_{i,j}) \\
dist_{i,j} &= ||\mathbf{c}_i - \mathbf{c}_j||
\end{aligned}
\qquad \text{Equation 4}
$$

where $f(\cdot)$ and $g(\cdot)$ were the neural networks. $P_{i,j}^{(l)} \in \mathbb{R}$ and $\alpha_{i,j}^{(l)} \in \mathbb{R}$ indicate the potential volume and interaction factor between the *i*-th and *j*-th atoms at the *l*-th hidden layer, respectively. $dist_{i,j} \in \mathbb{R}$ was the Euclidean distance between the *i*-th and *j*-th atoms. Thus, the atom interaction embeddings for the odorant ($\mathbf{x}_{\mathcal{O}} \in \mathbb{R}^d$) could be calculated by:

$$
\mathbf{x}_{\mathcal{O}} = \mathrm{Aggregate}(\{\mathbf{v}_i\}_{i=1}^{\mathcal{N}_{atom}}) \qquad \text{Equation 5}
$$

where $\mathrm{Aggregate}(\cdot)$ was the aggregate function, which was mean pooling in the present study. As an option, we added a residual part to prevent the vanishing gradient problem in the DNN (res-AINN), which could be defined as follows:

$$
\mathbf{v}_i^{(l+1)} = Norm(f(\mathbf{v}_i^l) + \sum_{j \in \mathcal{O} \setminus i} g(\mathbf{v}_j^{(l)}, P_{i,j}^{(l)}, \alpha_{i,j}^{(l)}) + \mathbf{v}_i^l) \qquad \text{Equation 6}
$$

Finally, the odorant embeddings $\mathbf{X}_{\mathcal{O}} = \{\mathbf{x}_{\mathcal{O}_i}\}_{i=1}^{\mathcal{N}_{sample}}$ were selected as inputs for subsequent models. In this study, the hyper-parameters *L*, dimensions of embeddings *d*, learning rate η, and learning epochs were selected as 6, {32, 64, 128, 256, 512, 1024}, 0.001, and 200, respectively. We considered the feasibility of using molecular 2D and 3D coordinates, and discussed the embedding results. Detailed information regarding atom interaction embedding can be found in other publications[27].

Results and Discussion

Data analysis

We employed five different molecular structure representations, including odorant molecular parameters (MP), molecular fingerprints (FP), pre-trained molecular graphic embeddings, pre-trained molecular graph transformer embeddings, and atom interaction embeddings in the present study. First, we visualized the numeric vectors in low-dimensional space using Barnes-Hut t-distributed stochastic neighbor embedding (t-SNE) as an unsupervised statistical method. This method has been widely applied for high-dimensional data visualization[50]. The t-SNE presentation of the odorants based on the above-mentioned vectors is illustrated in Figure 3 and Figure S1. As reported in previous studies, each odorant contained multi-odor category labels[14, 15, 24, 28]. Therefore, the distribution of odor categories was visualized using colors representing alpha values. Molecular graphic features extracted by Restnet (Figure 3c) produced a better result than other molecular features because most odorants from the same odor category are clustered together. In contrast, odor cluster overlapping was observed more frequently in the t-SNE map generated from molecular fingerprints (Figure 3a), molecular parameters (Figure 3b), and molecular graph transformers (Figure 3d). Molecular graphs generated from four combined types of pre-trained CNNs produced competitive results compared with other molecular descriptors (Figure S1). This result demonstrates that odor categories are likely to be more strongly related to molecular graphs than other descriptors. Therefore, we inferred that an odor category identification model based on molecular graphic features would be superior.

Molecular graphic CNN-based feature analysis

Figure 4 and Table S2 summarize the performance metrics of the odor category identification model based on molecular graphic feature extraction. The details of model calibration, including the optimal epochs, training loss, and elapsed time, are illustrated in Figure S2. The pre-trained RestNet with DNNs (6 hidden layers) performed significantly better than the other models, with the highest AUC (0.877±0.028, $p<0.001$) and F-score

227 (0.725±0.0278, p<0.001) on the test sets. It was followed by the DenseNet (4 hidden layers, AUC 0.876±0.029,
228 F-score 0.716±0.035), VGG (6 hidden layers, AUC 0.875±0.028, F-score 0.716±0.033), and AlexNet (5 hidden
229 layers, AUC 0.873±0.029, F-score 0.723±0.033). The deep residual framework of the most successful model may
230 have overcome the degradation problem that affects deep networks[40]. In addition, the number of hidden layers
231 in the DNN did not play a necessary role in tuning the pre-trained CNN model. To verify the abilities of the
232 models for transfer learning, we compared the prediction performances of the CNNs depending on whether
233 they were pre-trained. These results are illustrated in Figure 4. We found that the pre-trained models had
234 significantly (p<0.001) higher accuracy compared with the models with un-trained CNNs. This indicates that
235 CNNs could learn universal image feature extractors through training with a large dataset (ImageNet). This
236 conclusion is supported by previous research[51].

237 ***Molecular graph transformer based feature analysis***

238 A summary of the identification accuracy of the MGTNN models is given in Figure 5 and Table S3. The optimal
239 training epoch, loss, and elapsed time for the MGTNN models are presented in Figure S3. When the selected
240 atom and bond embeddings were included with 7 hidden layers, the MGTNN model had the highest AUC
241 (0.813±0.035) and F-score (0.696±0.032) in the test set. In addition, the AUC values for the models
242 independently trained via atom or bond embeddings were 0.812±0.031 and 0.810±0.030, respectively.
243 However, the data were not sufficient to conclude that considering atoms and bonds together produced a
244 significantly more accurate result than when they were included individually (p>0.001).

245 ***Atom interaction-based feature analysis***

246 Figure 6 and Table S4 compares odor sensory category identification according to the molecular features
247 extracted by AINNs. The results indicated that the AINN-DNN model (2D, 512 embedded dimensions) had the
248 highest identification performance in terms of the AUC and F-score, which were 0.807±0.035 (p<0.01) and
249 0.696±0.023, respectively. However, we cannot claim that the molecular 2D coordinates were better for

250 identification than the 3D coordinates because the analyses for both had a high p-value. Furthermore, the
251 models with residual modules did not exhibit a significant increase, likely because the vanishing gradient is not
252 the critical obstacle limiting AINN performance. In addition, the dimension of atom embedding vectors did not
253 have a significant effect on the accuracy of odor category identification. The optimal training epoch, loss, and
254 elapsed time for AINN models are listed in Figure S4. We found that the modeling time for 2D coordinates was
255 significantly smaller than that for 3D coordinates ($p<0.001$). This suggests that the presented AINN models do
256 not need spatial embedding for odor sensory identification.

257 ***Performance comparison***

258 To identify the model with the best comprehensive performance for odor category identification, we compared
259 the five types of models in terms of performance metrics, as presented in Figure 7 and Table 1. The predicted
260 accuracies for each odor sensory category are summarized in Figure S6-S10. The results confirmed that the
261 model trained using molecular graphic features extracted via a pre-trained ResNet had significantly better
262 performance than the other models (AUC 0.877±0.028, F-score 0.726±0.028, $p<0.0001$), followed by the AINN-
263 DNN (AUC 0.807±0.035, F-score 0.696±0.030), MPs (AUC 0.806±0.033, F-score 0.689±0.031), MGTNN (AUC
264 0.804±0.028, F-score 0.692±0.029), and FPs (AUC 0.796±0.036, F-score 0.688±0.033). This ranking could likely
265 be explained by the high correlation between the olfactory sensory information and the molecular graphic
266 features of the odorants compared with the other molecular descriptors. We found that the AINN-DNN model
267 had the highest precision (0.861±0.038, $p<0.0001$). Figure S5 illustrates the optimal training epoch, loss, and
268 elapsed time for the above-mentioned models. We confirmed that that although more epochs were needed to
269 train the ResNet models, the training time was shorter than that for the AINN-DNN and MGTNN models. The
270 fast convergence speed could contribute to the transfer-learning mechanism. Although the number of
271 parameters was abundant for the ResNet model, we did not train these parameters, but instead used those
272 from the pre-trained models. The pre-trained models could overcome the limitation of insufficient samples for
273 training DNN models. A similar conclusion was found previously[52]. In summary, we suggest that an end-to-end

274 DNN with molecular graphic features extracted via a pre-trained ResNet is an optimal model for predicting the
275 sensory categories of odorants.

276 ***Discussion***

277 The accurate and effective prediction of odor sensory categories is vital for developing machine-learning-based
278 GC/O. To develop an olfaction-based sensory system, we need not only bio-sensors to encode odorants (odor
279 receptor imitation), but also a brain-like odor signal decoding algorithm. Although many studies have examined
280 SORs, most have focused on predicting ODs[14, 15, 17, 20, 29]. Even though most ODs can be predicted, infrequent
281 ODs were difficult to be identified. For excample, Snitz proposed a mostly perfect result in prediciting 64 smell
282 percepts with 100% precision and 102 smells with 90.35%, but infrequent smells, such as almond, apricot and
283 chocolate, had been found to have poor prediction performance[15]. This could be explained by the extreme
284 imbalance in the data distribution, as well as the insufficient number of training samples. Unlike the above-
285 mentioned studies, we want to find useful odorant structure features for odor sensory categories
286 indentification.

287 Here, we focused on establishing relationships between molecular features and odor sensory categories via an
288 end-to-end learning strategy, which is expected to play a decoding role in bio-olfaction. The MPs and FPs in the
289 present study had poor performance, indicating that focusing solely on physiology-chemical parameters could
290 result in the loss of some critical information related to olfaction. In contrast to relying on tabular features,
291 molecular graph CNNs-based features would be more appropriate for learning useful odor sensory expression.
292 We also considered a transfer learning strategy for dealing with the problem of insufficient training samples.
293 Our results confirm that pre-trained CNNs, combined with a 'vanilla' DNN, can effectively establish relationships
294 between molecular features and odor sensory categories. Furthermore, our data suggest that molecular
295 graphic features are optimal for describing odorant protein interactions according to human olfaction. Existing
296 GC/O methods have focused on just 8 ODs in one olfaction sensory evaluation task, as limited by the odor

297 memory of the assessors[53-55]. Odor analysis precision is also limited by their odor memory. Therefore, the
298 proposed model can apply a reliable references for human panlists to reduce trainning cost.

299 This study has several limitations. First, more attention should be focused on atom interaction-based
300 embeddings, although the AINN in the present study had poor performance. Biological studies have indicated
301 that atom interactions play a critical role in mammal olfaction[56, 57]. The poor accuracy of the AINN was likely
302 caused by insufficient odorants and an inappropriate modeling approach. Moreover, we did not consider the
303 electronic interactions between atoms, which may be suitable for olfaction sensory encoding. Self-supervised
304 strategies combined with proper modeling techniques and trained with abundant molecules merit further
305 investigation. Furthermore, synergism, odor neutralization and the predicatable of a fragrance mixture has still
306 not been quantified[11, 58-60]. In present study, we focus on single odor molecule smell perception prediction,
307 which is not appropriate for modeling odor synergism and neutralization. For fragrance mixture prediction,
308 mass spectral would be feasible for model calibration. In the future, we plan to attempt to improve our
309 framework for molecular structure feature extraction using other algorithms, and to try to explore the feasibility
310 of metric modeling using Riemannian manifolds, such as the Grassmann or symmetric positive definite
311 manifold[61, 62]. We expect that it will be difficult to find a reasonable algorithm when performing metric learning
312 in Riemannian space. However, this is an interesting problem for future investigation. In addtion, data fusion
313 would also be an effective strategy for increasing the accurcay of odor category identification models.

314 Conclusion

315 The SOR by DNNs via the structure features of odorants has attracted great attention during the past decade.
316 Due to the limited knowledge on binding mechanism between odorant molecules and olfactory receptors,
317 however, it is not sure what kind of structural features play the most important role in smell recognition. Here,
318 we utilized a DNN-based multi-label classifier for odor sensory category identification using various molecular
319 features. Specifically, we examined the possibility of predicting odor categories based on molecular parameters,

fingerprints, and graphics, as well as graph attention network embedding and atom interactions. Our results indicated that molecular 2D graphic data were strongly related to sensory information about olfaction. Extensive experiments confirmed that a 'vanilla' DNN with molecular graphic features, extracted via ResNet, was optimal for odor perception category identification. We anticipate that transfer learning is a viable and powerful technique for modeling the relationships between molecular structures and odor perception categories. Our proposed approach could be applied in the development of AI-based odor sensors. We believe that this study is among the first to examine the importance of molecular graphic features when establishing relational models between molecular structures and odor sensory categories. Our approach may not only serve as a realistic solution for introducing AI into olfactometry, but may also offer a novel perspective for investigating the mechanisms of human olfaction.

Supporting Information

Supporting Information is available and includes model hyper parameter tunning and detail information for odor sensory categories.

Conflict of Interest

There is no conflict of interest to report.

Funding Information

This research was supported by China Postdoctoral Science Foundation (2021M703399), the National Key Research and Development Program of China (No. 2020YFB13400), National Nature Science Foundation of China (No. 61803369 and 61801400), and JSPS KAKENHI Grant (No. 18H03782).

References

1. Maurya, A.; Prasad, J.; Das, S.; Dwivedy, A. K., Essential oils and their application in food safety. *Front. Sustain. Food Syst.* **2021,** *5*.
2. Acree, T. E., GC/Olfactometry GC With a Sense of Smell. *Anal. Chem.* **1997,** *69* (5), 170A-175A.
3. Zhang, M.; Yu, H.; Zou, Q.; Li, Z.-A.; Lai, Y.; Cai, L.; Yin, P., Unique Ligand Exchange Dynamics of Metal－Organic Polyhedra for Vitrimer-like Gas Separation Membranes. *CCS Chem. 0* (0), 1-10.
4. Xue, C.; Liu, M.; Zhang, Z.-A.; Han, J.; Wang, C.; Wang, L.; Xiao, Z.; Zhu, W.-H., Controllable Fragrance Release Mediated by Spontaneous Hydrogen Bonding with POSS－Thiourea Derivatives. *CCS Chem. 2* (6), 478-487.
5. Barwich, A.-S., What makes a discovery successful? The story of linda buck and the olfactory receptors. *Cell* **2020,** *181* (4), 749-753.
6. Mori, K.; Takahashi, Y. K.; Igarashi, K. M.; Yamaguchi, M., Maps of odorant molecular features in the mammalian olfactory bulb. *Physiol. Rev.* **2006,** *86* (2), 409-433.
7. Haddad, R.; Lapid, H.; Harel, D.; Sobel, N., Measuring smells. *Curr. Opin. Neurobiol.* **2008,** *18* (4), 438-444.
8. Liu, C.; Miyauchi, H.; Hayashi, K., DeepSniffer: A meta-learning-based chemiresistive odor sensor for recognition and classification of aroma oils. *Sens. Actuators B Chem.* **2022,** *351*, 130960.
9. Chacko, R.; Jain, D.; Patwardhan, M.; Puri, A.; Karande, S.; Rai, B., Data based predictive models for odor perception. *Sci. Rep.* **2020,** *10* (1), 17136.
10. Shang, L.; Liu, C.; Tomiura, Y.; Hayashi, K. In *Artificial odor cluster map of odorant molecular parameters and odor maps in rat olfactory bulbs*, Chemical Senses, 2016; pp E212-E212.
11. Liu, S.; Zhang, J.; Liu, X.; Zhang, Y.; Zheng, Y.; Yuan, J.; Bao, J., Excitation wavelength as additional dimension in cross-reactive sensor arrays. *Sens. Actuators B Chem.* **2021,** *344*, 130183.
12. Nozaki, Y.; Nakamoto, T., Predictive modeling for odor character of a chemical using machine learning combined with natural language processing. *PLoS ONE* **2018,** *13* (6), e0208962.
13. Snitz, K.; Perl, O.; Honigstein, D.; Secundo, L.; Ravia, A.; Yablonka, A.; Endevelt-Shapira, Y.; Sobel, N., Smellspace: An odor-based social network as a platform for collecting olfactory perceptual data. *Chem. Senses* **2019,** *44* (4), 267-278.
14. Kumar, R.; Kaur, R.; Auffarth, B.; Bhondekar, A. P., Understanding the odour spaces: A step towards solving olfactory stimulus-percept problem. *PLOS ONE* **2015,** *10* (10), 1-19.
15. Snitz, K.; Yablonka, A.; Weiss, T.; Frumin, I.; Khan, R. M.; Sobel, N., Predicting odor perceptual similarity from odor structure. *PLoS Comput. Biol.* **2013,** *9* (9), e1003184.
16. Liu, C.; Shang, L.; Hayashi, K. In *Co-occurrence-based clustering of odor descriptors for predicting structure-odor relationship*, IEEE International Symposium on Olfaction and Electronic Nose (ISOEN), 2019; pp 1-4.
17. Loetsch, J.; Kringel, D.; Hummel, T., Machine learning in human olfactory research. *Chem. Senses* **2019,** *44* (1), 11-22.

18. Esme, E.; Kiran, M. S. In *The performance analysis of extreme learning machines on odour recognition*, Proceedings of the 2018 2nd International Conference on Cloud and Big Data Computing, New York, NY, USA, Association for Computing Machinery: New York, NY, USA, 2018; pp 87-92.
19. Choi, Y.; Kim, K.; Kim, S.; Kim, D., Identification of odor emission sources in urban areas using machine learning-based classification models. *Atmos* **2022,** *13*, 100156.
20. Debnath, T.; Nakamoto, T., Predicting human odor perception represented by continuous values from mass spectra of essential oils resembling chemical mixtures. *PLoS ONE* **2020,** *15* (6), e0234688.
21. Hasebe, D.; Nakamoto, T. In *A model to predict mass spectrum from odor impression using deep neural network*, 2021 IEEE Sensors, 2021; pp 1-4.
22. Liu, Q.; Luo, D.; Wen, T.; GholamHosseini, H.; Qiu, X.; Li, J., POI-3DGCN: Predicting odor intensity of monomer flavors based on three-dimensionally embedded graph convolutional network. *Expert Syst. Appl.* **2022**, 116997.
23. Gutiérrez, E. D.; Dhurandhar, A.; Keller, A.; Meyer, P.; Cecchi, G. A., Predicting natural language descriptions of mono-molecular odorants. *Nat. Commun.* **2018,** *9* (1), 4979.
24. Shang, L.; Liu, C. J.; Tomiura, Y.; Hayashi, K., Machine-learning-based olfactometer: Prediction of odor perception from physicochemical features of odorant molecules. *Anal. Chem.* **2017,** *89* (22), 11999-12005.
25. Dravnieks, A., Odor quality: Semantically generated multidimensional profiles are stable. *Science* **1982,** *218* (4574), 799-801.
26. Shang, L.; Liu, C.; Chen, B.; Tang, F.; Liu, L.; Hayashi, K., Machine-learning-based olfactometry: Odor descriptor clustering based on bayesian embedding model and its prediction from molecular graphic features. *Submitted* **2021**.
27. Tsubaki, M.; Mizoguchi, T., Fast and accurate molecular property prediction: learning atomic interactions and potentials with neural networks. *J. Phys. Chem.* **2019,** *10* (9), 2066-2067.
28. Snchez-Lengeling, B.; Wei, J. N.; Lee, B. K.; Gerkin, R. C.; Aspuru-Guzik, A.; Wiltschko, A. B., Machine learning for scent: Learning generalizable perceptual representations of small molecules. *ArXiv* **2019,** *abs/1910.10685*.
29. Sharma, A.; Kumar, R.; Ranjta, S.; Varadwaj, P. K., SMILES to smell: Decoding the structure-odor relationship of chemical compounds using the deep neural network approach. *J. Chem. Inf. Model.* **2021,** *61* (2), 676-688.
30. Johnson, B. A.; Xu, Z.; Ali, S. S.; Leon, M., Spatial representations of odorants in olfactory bulbs of rats and mice: Similarities and differences in chemotopic organization. *J. Comp. Neurol.* **2009,** *514* (6), 658-673.
31. Sigma-Aldrich, Flavors and fragrances products catalog. *Merck KGaA: Darmstadt* **2016**.
32. Arn, H.; Acree, T. E.; Contis, E. T.; Ho, C.-T.; Mussinan, C. J.; Parliment, T. H.; Shahidi, F.; Spanier, A. M., Flavornet: A database of aroma compounds based on odor potency in natural products. In *Developments in Food Science*, Elsevier: 1998; Vol. 40, p 27.
33. Landrum, G., Open-source cheminformatics. *GitHub and SourceForge* **2012,** *3* (4).
34. Kim, S.; Chen, J.; Cheng, T.; Gindulyte, A.; He, J.; He, S.; Li, Q.; Shoemaker, B. A.; Thiessen, P. A.; Yu,

411 B.; Zaslavsky, L.; Zhang, J.; Bolton, E. E., PubChem in 2021: New data content and improved web interfaces.
412 *Nucleic Acids Res.* **2021,** *49* (D1), D1388-D1395.
413 35. Moriwaki, H.; Tian, Y.-S.; Kawashita, N.; Takagi, T., Mordred: a molecular descriptor calculator. *J.*
414 *Cheminformatics* **2018,** *10* (1), 4.
415 36. Wang, J.-L.; Wu, H.-N.; Huang, T.; Xu, M., Output synchronization in coupled neural networks with and without
416 external disturbances. *IEEE Trans. Control. Netw. Syst.* **2018,** *5* (4), 2049-2061.
417 37. Zhang, T.; Waqas, M.; Liu, Z.; Tu, S.; Halim, Z.; Rehman, S. U.; Li, Y.; Han, Z., A fusing framework of
418 shortcut convolutional neural networks. *Inf. Sci.* **2021,** *579*, 685-699.
419 38. Krizhevsky, A.; Sutskever, I.; Hinton, G. E., imagenet classification with deep convolutional neural networks.
420 *Commun. ACM* **2017,** *60* (6), 84-90.
421 39. Huang, G.; Liu, Z.; Van Der Maaten, L.; Weinberger, K. Q. In *Densely connected convolutional networks*, IEEE
422 Conference on Computer Vision and Pattern Recognition (CVPR), 2017; pp 2261-2269.
423 40. He, K.; Zhang, X.; Ren, S.; Sun, J. In *Deep residual learning for image recognition*, Proceedings of the IEEE
424 Conference on Computer Vision and Pattern Recognition, 2016; pp 770-778.
425 41. Simonyan, K.; Zisserman, A. In *Very deep convolutional networks for large-scale image recognition*,
426 International Conference on Learning Representations (ICLR), 2015.
427 42. Mei, X.; Cai, X.; Yang, L.; Wang, N., Graph transformer networks based text representation. *Neurocomputing*
428 **2021,** *463*, 91-100.
429 43. Warikoo, N.; Chang, Y.-C.; Hsu, W.-L., LBERT: Lexically aware transformer-based bidirectional encoder
430 representation model for learning universal bio-entity relations. *Bioinformatics* **2021,** *37* (3), 404-412.
431 44. Rong, Y.; Bian, Y.; Xu, T.; Xie, W.; Ying, W. E. I.; Huang, W.; Huang, J. In *Self-supervised graph transformer*
432 *on large-scale molecular data*, Adv. Neural Inf. Process. Syst., Larochelle, H.; Ranzato, M.; Hadsell, R.; Balcan,
433 M. F.; Lin, H., Eds. Curran Associates, Inc.: 2020; pp 12559-12571.
434 45. Chen, D.; Gao, K.; Nguyen, D. D.; Chen, X.; Jiang, Y.; Wei, G.-W.; Pan, F., Algebraic graph-assisted
435 bidirectional transformers for molecular property prediction. *Nat. Commun.* **2021,** *12* (1), 3521.
436 46. Mao, K.; Xiao, X.; Xu, T.; Rong, Y.; Huang, J.; Zhao, P., Molecular graph enhanced transformer for
437 retrosynthesis prediction. *Neurocomputing* **2021,** *457*, 193-202.
438 47. Fjaeldstad, A.; Fernandes, H. M.; Van Hartevelt, T. J.; Gleesborg, C.; Møller, A.; Ovesen, T.; Kringelbach, M.
439 L., Brain fingerprints of olfaction: a novel structural method for assessing olfactory cortical networks in health
440 and disease. *Sci. Rep.* **2017,** *7* (1), 42534.
441 48. Fjaeldstad, A., Testing olfactory function and mapping the structural olfactory networks in the brain. *Dan. Med.*
442 *J.* **2018,** *65*.
443 49. Chen, L.; Tan, X.; Wang, D.; Zhong, F.; Liu, X.; Yang, T.; Luo, X.; Chen, K.; Jiang, H.; Zheng, M.,
444 TransformerCPI: Improving compound-protein interaction prediction by sequence-based deep learning with self-
445 attention mechanism and label reversal experiments. *Bioinformatics* **2020,** *36* (16), 4406-4414.
446 50. Shang, L.; Liu, C. J.; Tomiura, Y.; Hayashi, K., Odorant clustering based on molecular parameter-feature

extraction and imaging analysis of olfactory bulb odor maps. *Sens. Actuators B Chem.* **2018,** *255*, 508-518.

51. Liu, C.; Liu, P.; Zhao, W.; Tang, X., Visual tracking by structurally optimizing pre-trained CNN. *IEEE Trans. Circuits. Syst. Video Technol.* **2020,** *30* (9), 153-3166.
52. Pezzotti, N.; Lelieveldt, B. P. F.; van der Maaten, L.; Hollt, T.; Eisemann, E.; Vilanova, A., Approximated and user steerable tSNE for progressive visual analytics. *IEEE Trans. Vis. Comput. Graph.* **2017,** *23* (7), 1739-1752.
53. Brattoli, M.; Cisternino, E.; Dambruoso, P. R.; de Gennaro, G.; Giungato, P.; Mazzone, A.; Palmisani, J.; Tutino, M., Gas chromatography analysis with olfactometric detection (GC-O) as a useful methodology for chemical characterization of odorous compounds. *Sens.* **2013,** *13* (24316571), 16759-16800.
54. Aznar, M.; López, R.; Cacho, J. F.; Ferreira, V., Identification and quantification of impact odorants of aged red wines from Rioja. GC−Olfactometry, quantitative GC-MS, and odor evaluation of HPLC fractions. *J. Agric. Food Chem.* **2001,** *49* (6), 2924-2929.
55. Vene, K.; Seisonen, S.; Koppel, K.; Leitner, E.; Paalme, T., A method for GC-Olfactometry panel training. *Chemosensory Perception* **2013,** *6* (4), 179-189.
56. Ma, H.; Wang, T.; Li, B.; Cao, W.; Zeng, M.; Yang, J.; Su, Y.; Hu, N.; Zhou, Z.; Yang, Z., A low-cost and efficient electronic nose system for quantification of multiple indoor air contaminants utilizing HC and PLSR. *Sens. Actuators B Chem.* **2022,** *350*, 130768.
57. Mantel, M.; Fournel, A.; Staedlé, I.; Oelschlägel, A.; Carro, J.; Dubreuil, R.; Herrier, C.; Livache, T.; Haehner, A.; Hummel, T.; Roy, J.-M.; Bensafi, M., Using a bio-inspired surface resonance plasmon electronic nose for fundamental research on human olfaction. *Sens. Actuators B Chem.* **2022,** *350*, 130846.
58. Hudon, G.; Guy, C.; Hermia, J., Measurement of odor intensity by an electronic nose. *J. Air Waste Manag Assoc.* **2000,** *50*, 1750-1578.
59. Yan, L.; Liu, J.; Jiang, S.; Wu, C.; Gao, K., The regular interaction pattern among odorants of the same type and its application in odor intensity assessment. *Sensors* **2017,** *17* (7), 1624.
60. Zhang, L.; Mao, H.; Zhuang, Y.; Wang, L.; Liu, L.; Dong, Y.; Du, J.; Xie, W.; Yuan, Z., Odor prediction and aroma mixture design using machine learning model and molecular surface charge density profiles. *Chem. Eng. Sci.* **2021,** *245* (14), 116947.
61. Tang, F.; Feng, H.; Tino, P.; Si, B.; Ji, D., Probabilistic learning vector quantization on manifold of symmetric positive definite matrices. *Neural Netw.* **2021,** *142*, 105-118.
62. Matsukawa, T.; Okabe, T.; Suzuki, E.; Sato, Y., Hierarchical Gaussian descriptors with application to person re-identification. *IEEE Trans. Pattern Anal. Mach. Intell.* **2020,** *42* (9), 2179-2194.

Table of Contents Graphic

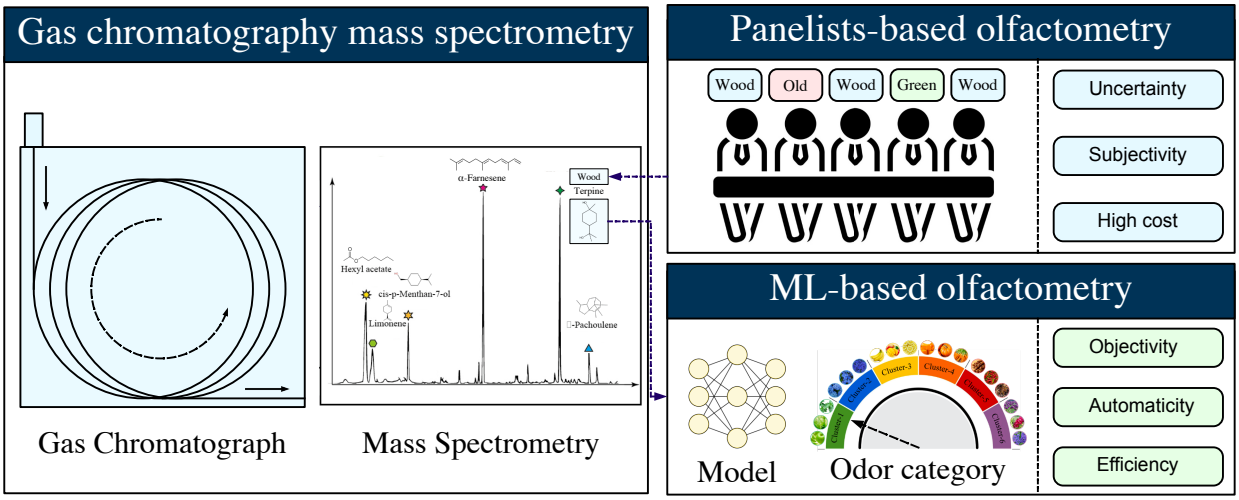

Figure captions

Figure 1. Data processing for calibration and validation of an odor category prediction model.

Figure 2. Overview of the design of molecular feature extractors, including (a) a molecular graphic convolution neural network (MG-CNN), (b) molecular graph transformer neural network (MGT-NN), and (c) atom interaction neural network (AINN).

Figure 3. Odorant clustering using Barnes-Hut t-distributed stochastic neighbor embedding (t-SNE) based on (a) molecular fingerprints, (b) molecular parameters, and (c) molecular graphic features extracted via a pre-trained Restnet and (d) molecular graph transformer method based on the links between atoms and bonds. tSNE-1 and tSNE-2 were calculated using the t-SNE method. Each point indicates an odorant, colored according to its odor category labels, and the distributions of odor categories are given by the alpha values corresponding to the colors.

492 **Figure 4.** Identification performance of four molecular graphic convolution neural network (MG-
493 CNN) models: AlexNet, VGG, DenseNet, and ResNet. The models were evaluated according to the
494 average identification AUC (a), precision (b), recall (c), and F-score (d). Results were evaluated
495 using the nonparametric Wilcoxon signed-rank test.

496 **Figure 5.** Determination of odor category by molecular graph transformer neural network
497 (MGTNN) models for atom embeddings only, bond embeddings only, and combinations thereof.
498 Models were evaluated according to the average identification AUC (a), precision (b), recall (c),
499 and F-score (d). Results were subjected to the nonparametric Wilcoxon signed-rank test.

500 **Figure 6.** Results for odor category determined by atom interaction neural network (AINN) models.
501 The models were evaluated according to the average identification area under the curve (AUC)
502 (a), precision (b), recall (c), and F-score (d). The data were subjected to a nonparametric Wilcoxon
503 signed-rank test.

504 **Figure 7.** Identification accuracies of DNN models using molecular features extracted via FP-, MP-,
505 MG-CNN-, MGTNN-, and AINN-based DNN models. The data were evaluated using the
506 nonparametric Wilcoxon signed-rank test.
507

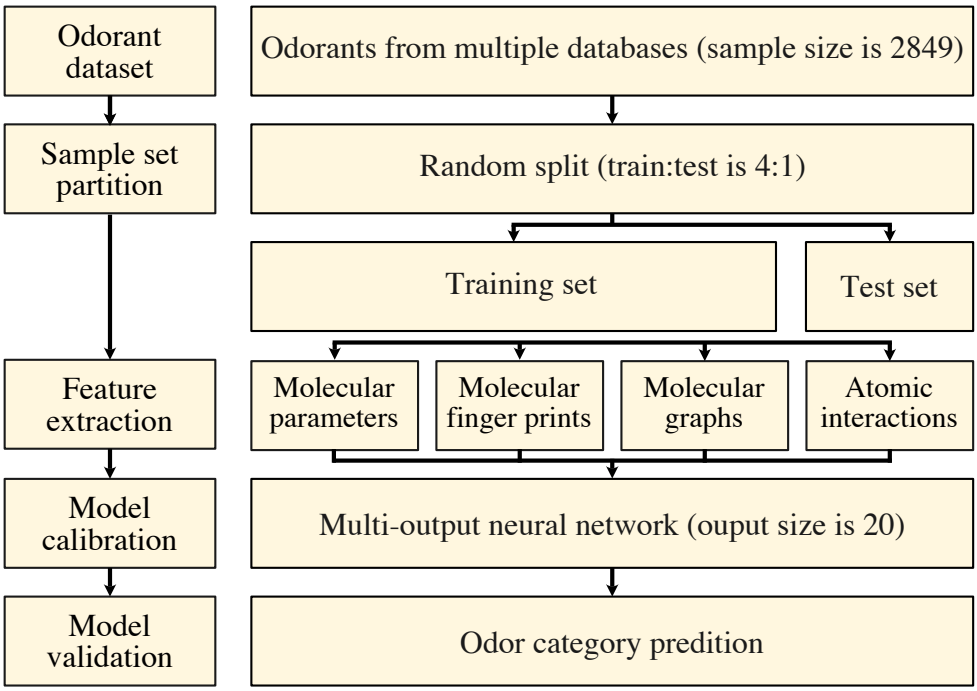
Odorant dataset
Odorants from multiple databases (sample size is 2849)
Sample set partition
Random split (train:test is 4:1)
Training set
Test set
Feature extraction
Molecular parameters
Molecular finger prints
Molecular graphs
Atomic interactions
Model calibration
Multi-output neural network (ouput size is 20)
Model validation
Odor category predition

Figure 1.

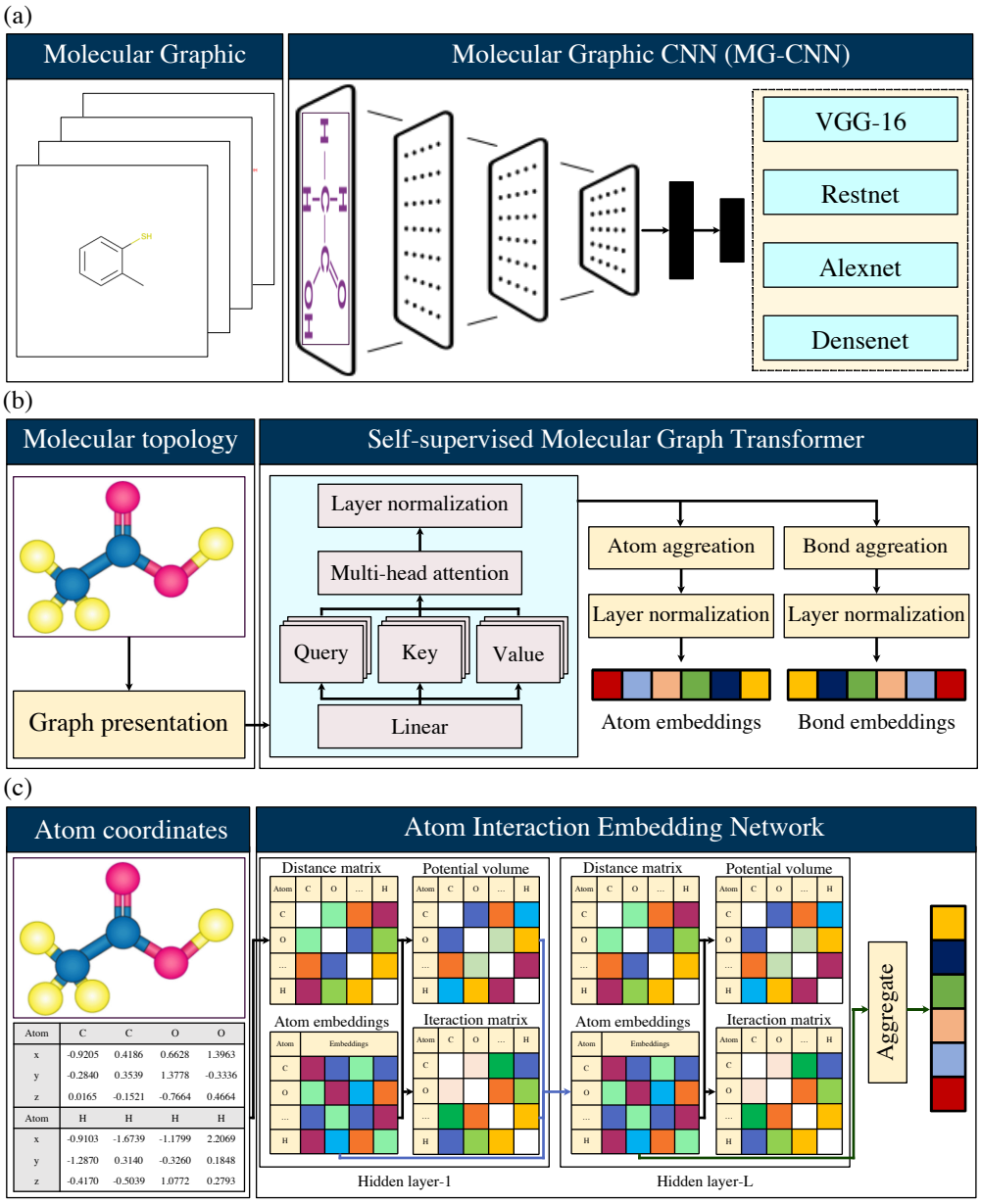
(a)
Molecular Graphic
Molecular Graphic CNN (MG-CNN)
VGG-16
Restnet
Alexnet
Densenet
(b)
Molecular topology
Self-supervised Molecular Graph Transformer
Graph presentation
Layer normalization
Multi-head attention
Query
Key
Value
Linear
Atom aggreation
Bond aggreation
Layer normalization
Layer normalization
Atom embeddings
Bond embeddings
(c)
Atom coordinates
Atom Interaction Embedding Network
Distance matrix
Potential volume
Atom embeddings
Iteraction matrix
Hidden layer-1
Hidden layer-L
Aggregate

Figure 2.

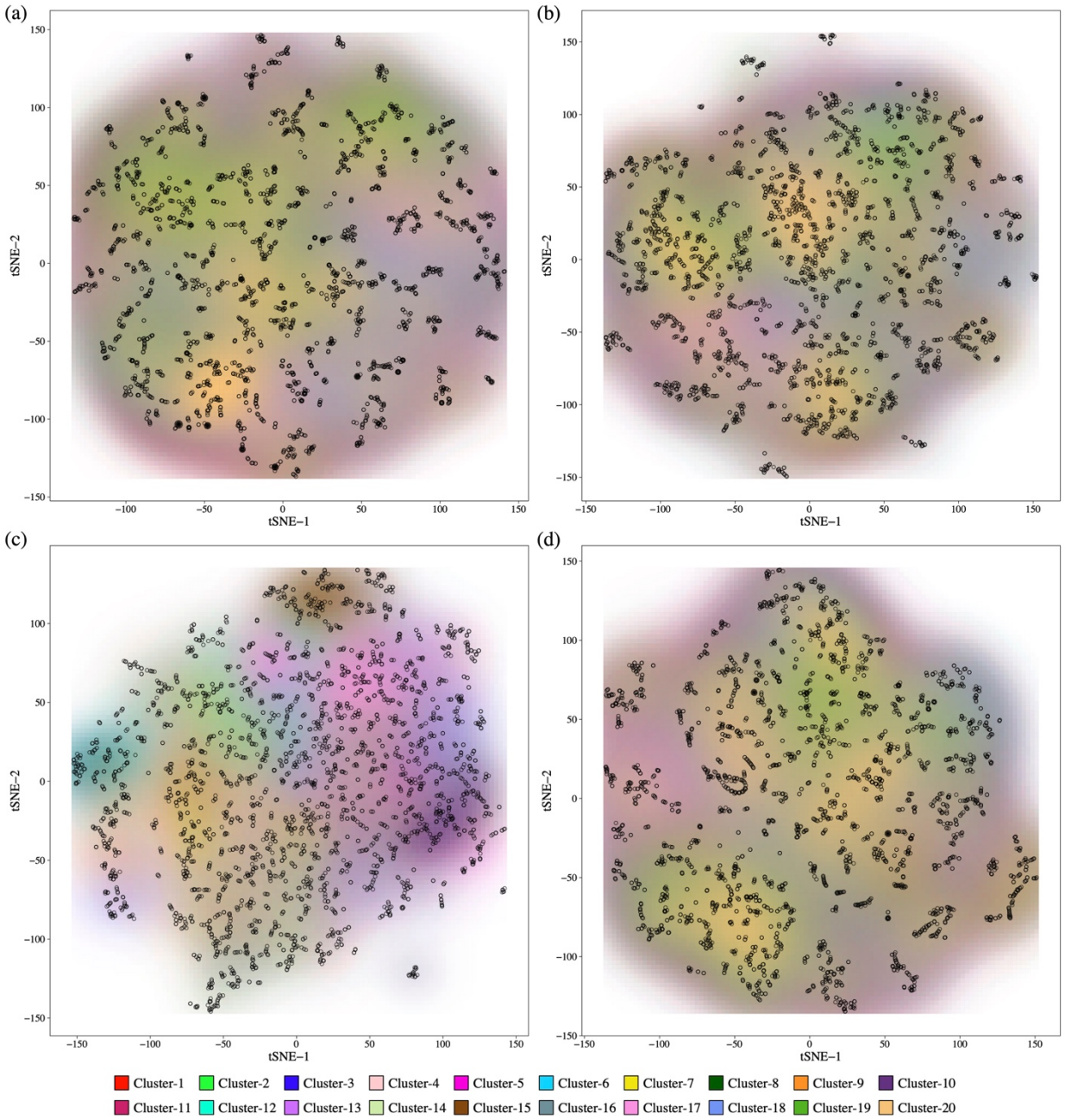
(a)
(b)
(c)
(d)
tSNE−1
tSNE−2
Cluster-1
Cluster-2
Cluster-3
Cluster-4
Cluster-5
Cluster-6
Cluster-7
Cluster-8
Cluster-9
Cluster-10
Cluster-11
Cluster-12
Cluster-13
Cluster-14
Cluster-15
Cluster-16
Cluster-17
Cluster-18
Cluster-19
Cluster-20

Figure 3.

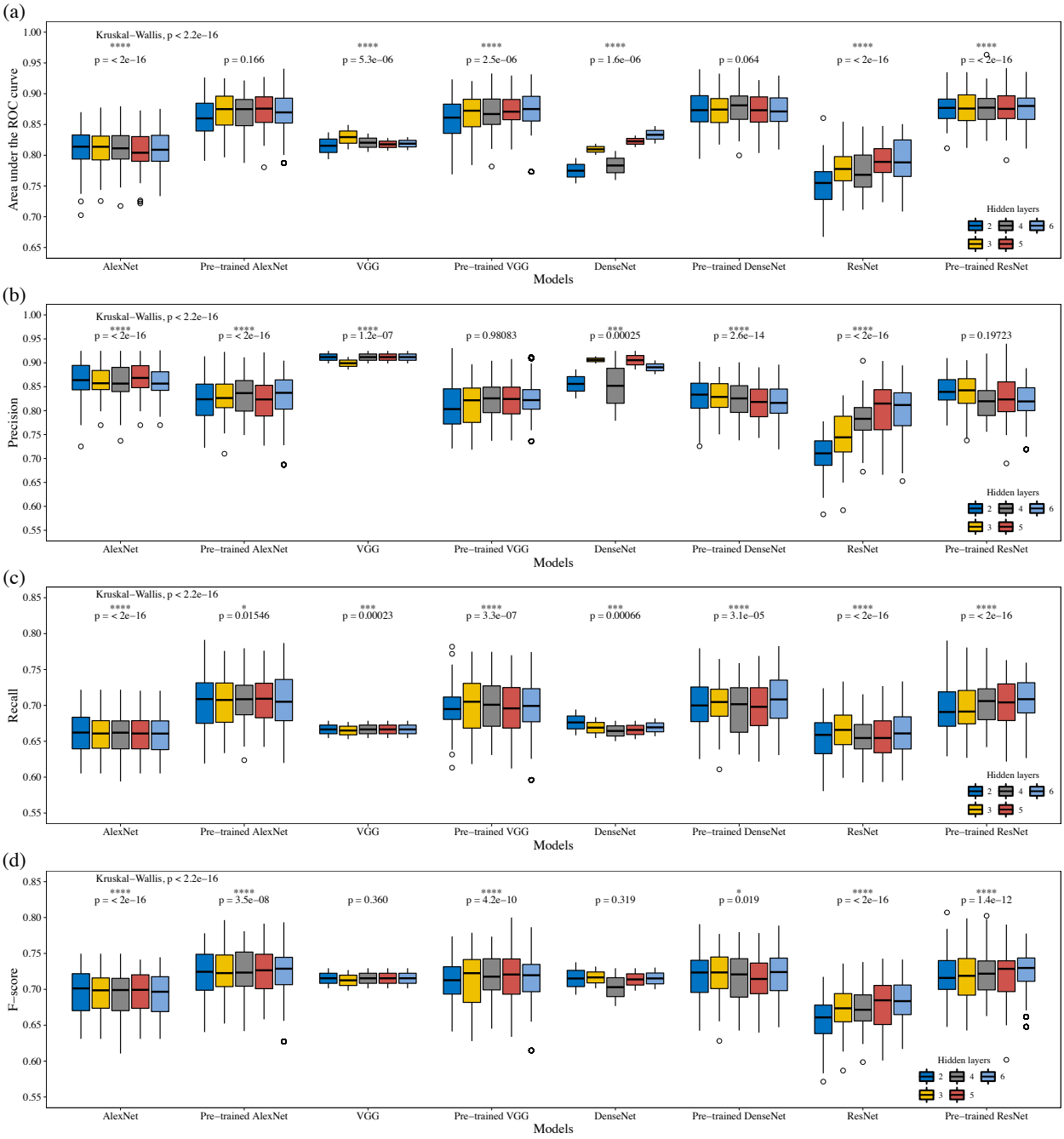
(a)
Kruskal–Wallis, p < 2.2e–16
Area under the ROC curve
p = < 2e–16
p = 0.166
p = 5.3e–06
p = 2.5e–06
p = 1.6e–06
p = 0.064
p = < 2e–16
p = < 2e–16
Hidden layers
2 4 6
3 5
AlexNet
Pre–trained AlexNet
VGG
Pre–trained VGG
DenseNet
Pre–trained DenseNet
ResNet
Pre–trained ResNet
Models
(b)
Kruskal–Wallis, p < 2.2e–16
Precision
p = < 2e–16
p = < 2e–16
p = 1.2e–07
p = 0.98083
p = 0.00025
p = 2.6e–14
p = < 2e–16
p = 0.19723
Models
(c)
Kruskal–Wallis, p < 2.2e–16
Recall
p = < 2e–16
p = 0.01546
p = 0.00023
p = 3.3e–07
p = 0.00066
p = 3.1e–05
p = < 2e–16
p = < 2e–16
Models
(d)
Kruskal–Wallis, p < 2.2e–16
F–score
p = < 2e–16
p = 3.5e–08
p = 0.360
p = 4.2e–10
p = 0.319
p = 0.019
p = < 2e–16
p = 1.4e–12
Models

Figure 4.

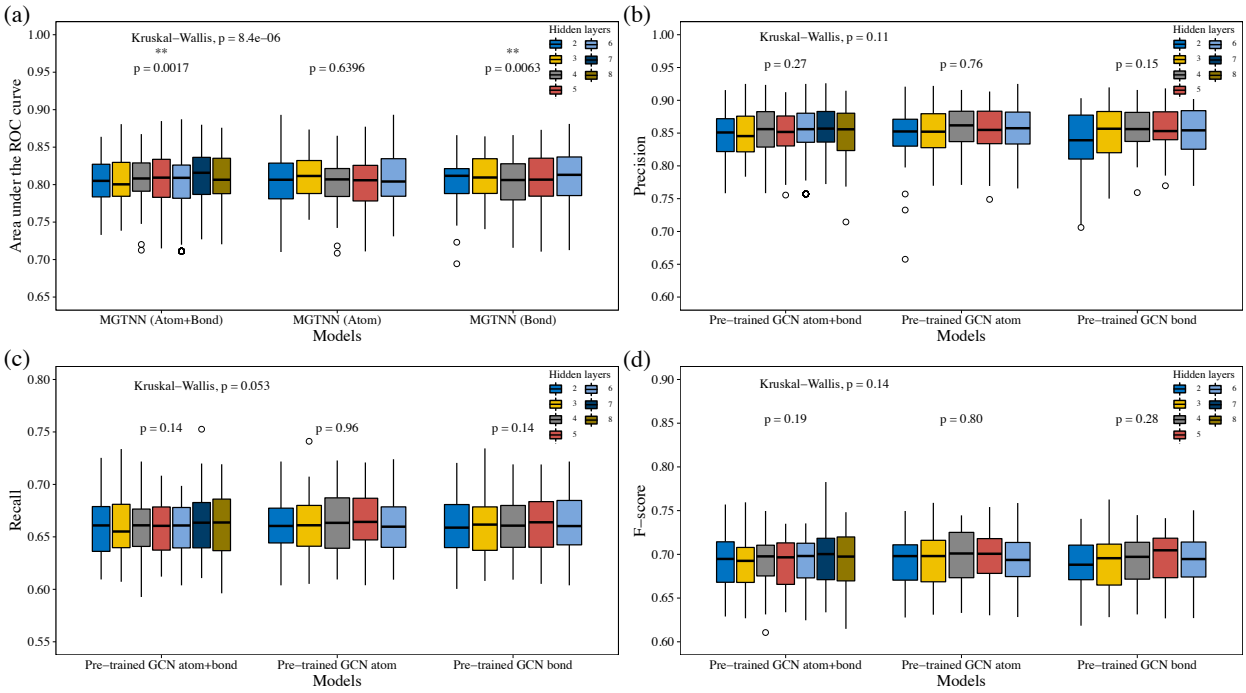
(a)
Kruskal−Wallis, p = 8.4e−06
**
p = 0.0017
p = 0.6396
**
p = 0.0063
Hidden layers
2 3 4 5 6 7 8
Area under the ROC curve
1.00 0.95 0.90 0.85 0.80 0.75 0.70 0.65
MGTNN (Atom+Bond)
MGTNN (Atom)
MGTNN (Bond)
Models
(b)
Kruskal−Wallis, p = 0.11
p = 0.27
p = 0.76
p = 0.15
Hidden layers
2 3 4 5 6 7 8
Precision
1.00 0.95 0.90 0.85 0.80 0.75 0.70 0.65 0.60
Pre−trained GCN atom+bond
Pre−trained GCN atom
Pre−trained GCN bond
Models
(c)
Kruskal−Wallis, p = 0.053
p = 0.14
p = 0.96
p = 0.14
Hidden layers
2 3 4 5 6 7 8
Recall
0.80 0.75 0.70 0.65 0.60 0.55
Pre−trained GCN atom+bond
Pre−trained GCN atom
Pre−trained GCN bond
Models
(d)
Kruskal−Wallis, p = 0.14
p = 0.19
p = 0.80
p = 0.28
Hidden layers
2 3 4 5 6 7 8
F−score
0.90 0.85 0.80 0.75 0.70 0.65 0.60
Pre−trained GCN atom+bond
Pre−trained GCN atom
Pre−trained GCN bond
Models

Figure 5.

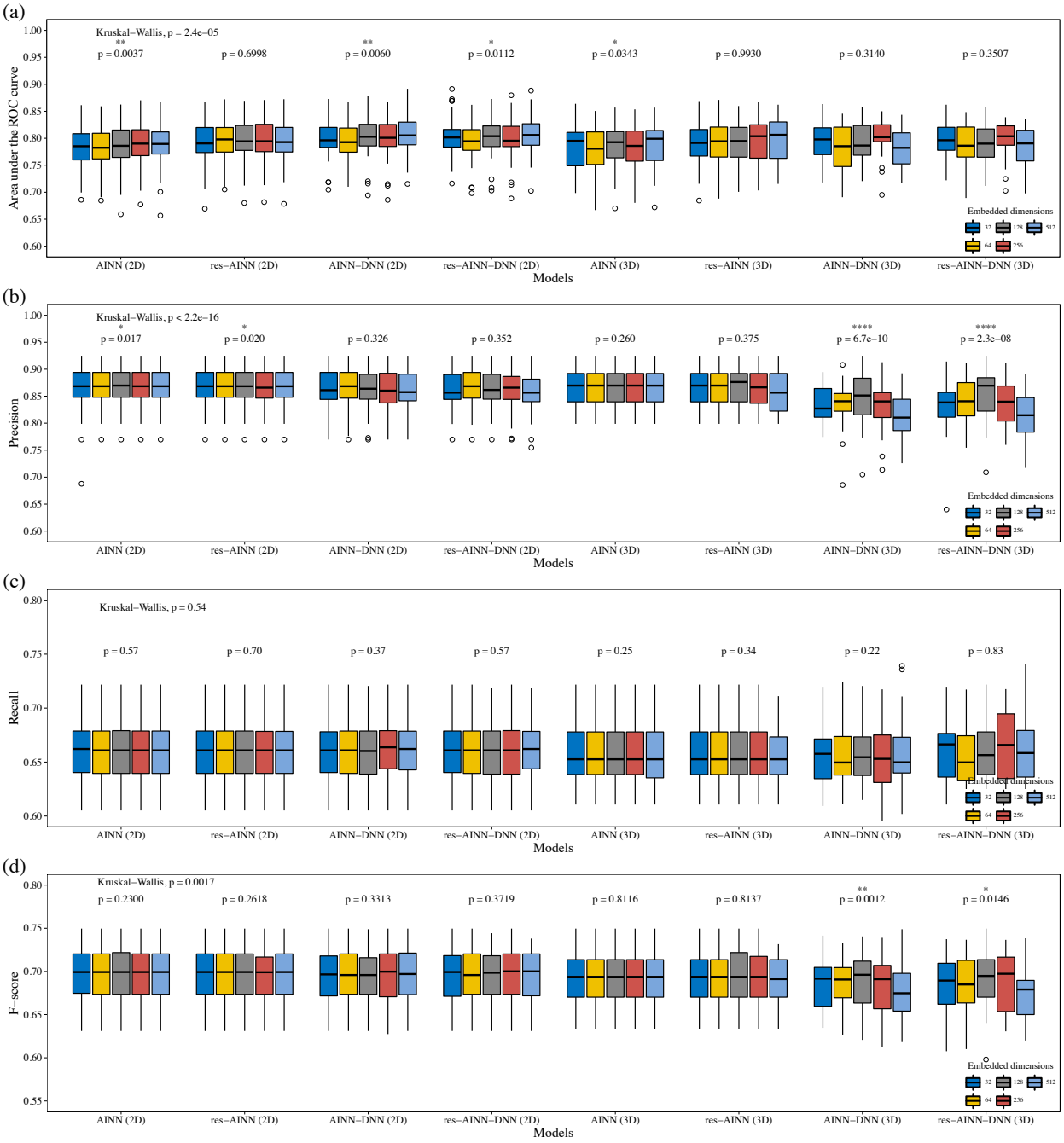
(a)
Kruskal–Wallis, p = 2.4e–05
p = 0.0037
p = 0.6998
p = 0.0060
p = 0.0112
p = 0.0343
p = 0.9930
p = 0.3140
p = 0.3507
Area under the ROC curve
Embedded dimensions
32
64
128
256
512
AINN (2D)
res–AINN (2D)
AINN–DNN (2D)
res–AINN–DNN (2D)
AINN (3D)
res–AINN (3D)
AINN–DNN (3D)
res–AINN–DNN (3D)
Models
(b)
Kruskal–Wallis, p < 2.2e–16
p = 0.017
p = 0.020
p = 0.326
p = 0.352
p = 0.260
p = 0.375
p = 6.7e–10
p = 2.3e–08
Precision
(c)
Kruskal–Wallis, p = 0.54
p = 0.57
p = 0.70
p = 0.37
p = 0.57
p = 0.25
p = 0.34
p = 0.22
p = 0.83
Recall
(d)
Kruskal–Wallis, p = 0.0017
p = 0.2300
p = 0.2618
p = 0.3313
p = 0.3719
p = 0.8116
p = 0.8137
p = 0.0012
p = 0.0146
F–score

Figure 6.

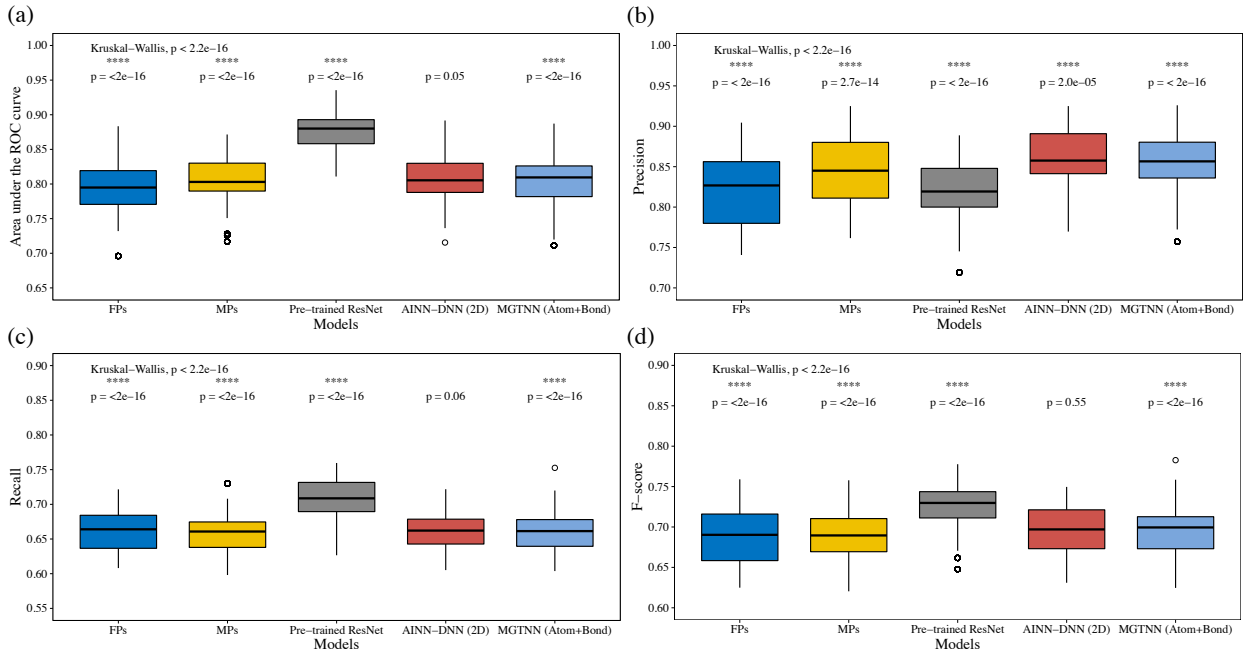

Figure 7.

Table captions

Table 1. Odor sensory category identification accuracy comparison of DNN models using multi-type of odorant structure features.

Model name	AUC-ROC	Precision	Recall	F-score
FP-based	0.796±0.036	0.82±0.046	0.662±0.029	0.688±0.033
MP-based	0.806±0.033	0.843±0.039	0.658±0.028	0.689±0.031
MG-CNN-based	0.877±0.028	0.822±0.037	0.71±0.028	0.726±0.028
MGT-NN-based	0.804±0.036	0.855±0.036	0.659±0.025	0.692±0.029
AINN-based	0.807±0.035	0.861±0.038	0.662±0.027	0.696±0.03